

„AL.I. CUZA” UNIVERSITY IAȘI
FACULTY of PHYSICS

Contributions to the study of nanoparticles with potential applications in targeted drug delivery

-ABSTRACT-

PhD student,

ALINA MIHAELA COJOCARIU

Scientific coordinator,

Prof. Dr. OVIDIU FLORIN CĂLȚUN

-Iași, 2013-



UNIUNEA EUROPEANĂ



GUVERNUL ROMÂNIEI
MINISTERUL ȘTIINȚELOR, INFORMATICII ȘI
INOVĂȚILOR



Fondul Social European
POS DRU 2007-2013



Instituția Națională de Cercetare
și Dezvoltare în Fizică
2007-2013



MINISTERUL
EDUCAȚIEI, CERCETĂRII
ȘTIINȚELOR ȘI SPORTULUI



UNIVERSITATEA
ALEXANDRU I. CUZA
IAȘI

„Alexandru Ioan Cuza” University Iași
To the attention of

.....

We would like to inform you that on the 26th of September 2013 at 12 o'clock, in room L1, the PhD student Alina Mihaela Cojocariu will present her thesis **“Contributions to the study of nanoparticles with possible applications in targeted drug delivery”** in order to obtain the degree of doctor in Physics.

The Committee will be composed of:

President: Prof. Dr. Diana Mardare, Faculty of Physics,
"Alexandru Ioan Cuza" University

Members: Prof. Dr. Ovidiu Florin CĂLȚUN, scientific
coordinator, “Alexandru Ioan Cuza” University, Iași

Prof. Dr. Aurel PUI – “Alexandru Ioan Cuza”
University, Iași

Prof. Dr. Viorica SIMON – “Babeș Bolyai”
University, Cluj Napoca

Prof. Dr. Rolf HEMPELMANN – Saarland
University, Saabrucken, Germany

We would like to invite you to attend the public
presentation of the PhD thesis.

*I would like to address my respectful thanks to **Prof. Dr. Ovidiu Florin Călțun**, my scientific coordinator for all of the confidence, patience and his constant guidance throughout the period of the doctoral study.*

Thanks to the entire examination committee for patience and for their time spent as referees for my PhD thesis.

*I also owe a special thank you to **Prof. Dr. Rolf Hempelmann** and his team from the University of Saarland, Germany, for welcoming me in his team and for offering me all the support to achieve the synthesis, functionalization and characterization of magnetic nanoparticles.*

*I also want to thank **Prof. Dr. Florin Brînză, Lect. Dr. Ioan Dumitru** and **Lect. Dr. Iordana Aștefănoaei** for the support provided and for the continuous discussions throughout the preparation of the thesis and for allowing me to use the materials and instruments needed during my study.*

*A debt of gratitude goes to **Prof. Dr. Aurel Pui** and my fellow PhD. Student **Daniel Ghercă**, for their support in investigating the interaction of the synthesized and functionalized nanoparticles with blood.*

*Thanks to all my colleagues from the **Faculty of Physics** both for the constructive discussions and for their moral support.*

This work was supported by the European Social Fund in Romania, under the responsibility of the Managing Authority for the Sectoral Operational Programme for Human Resources Development 2007-2013 [grant POSDRU/107/1.5/S/78342].

Special thanks to my family for all the unconditional support throughout the course of the doctoral studies, this success being dedicated to my parents. Particular thanks to my fiancé who trusted in me and supported me.

Table of contents

| | |
|---|----|
| Acknowledgement..... | 4 |
| Abstract..... | 5 |
| Chapter I. Current status of research on the methods of synthesis and the practical applications of nanosized drug delivery systems..... | 7 |
| I.1 Nanotechnology..... | 7 |
| I.2 Current status of research in nanoparticulate systems..... | 8 |
| I.3 Methods for synthesis of nanostructured systems..... | 11 |
| I.3.1 Co-precipitation method | 12 |
| I.3.2 Microemulsion method | 13 |
| I.3.3 Sol-gel method..... | 14 |
| I.3.4 Hydrothermal method..... | 14 |
| I.4 Applications of nanoparticles in medicine - targeted drug delivery..... | 15 |
| I.4.1 The principle of magnetic drug delivery..... | 18 |
| I.4.2 Groups of nanoparticles used in magnetic drug delivery | 21 |
| I.5 Conclusions..... | 27 |
| References..... | 28 |
| Chapter II. Methods of characterization and functionalization of nanoparticles..... | 33 |
| II.1 Characterization techniques..... | 33 |
| II.1.1 The method of X-ray diffractometer..... | 33 |
| II.1.2 Transmission electron microscopy (TEM) and spectroscopy by energy dispersion X radiation (EDX)..... | 36 |
| II.1.3 Dynamic light scattering (DLS)..... | 39 |
| II.1.4 Particle to particle analysis method (NTA)..... | 41 |
| II.1.5 Method for determining the zeta potential..... | 43 |
| II.1.6 Fourier Transform Infrared Spectroscopy..... | 44 |
| II.1.7 Vibrating sample magnetometer (VSM)..... | 45 |
| II.2 Methods for functionalization of nanoparticles for medical applications..... | 46 |
| II.2.1 Layer-by-layer deposition method (LbL)..... | 48 |
| References..... | 52 |
| Chapter III. Experimental results - Synthesis method and experimental techniques for studying the structural and magnetic properties of the obtained nanostructures..... | 54 |
| III.1 Obtaining magnetic nanostructures of $Zn_xCo_{1-x}Fe_2O_4$ | 54 |
| III.2 Characterization of magnetic nanoparticles $Zn_xCo_{1-x}Fe_2O_4$ series..... | 57 |
| III.2.1 The results of microstructure by X-ray diffraction..... | 57 |
| III.2.2 Study of microstructure and chemical composition using transmission electron microscopy (TEM) and X ray spectroscopy with energy dispersive (EDX)..... | 63 |
| III.2.3 The determination of the hydrodynamic diameter of the powder of the $Zn_xCo_{1-x}Fe_2O_4$ series..... | 66 |
| III.2.3.1 Dynamic light scattering method (DLS)..... | 66 |
| III.2.3.2 Particle to particle analysis method (NTA)..... | 67 |
| III.2.4 Zeta Potential determination for colloidal dispersions..... | 69 |
| III.2.5 Influence of chemical composition on IR spectra..... | 70 |

| | | |
|--------------------|---|------------|
| III.2.6 | Influence of chemical composition on the magnetic properties (VSM)..... | 72 |
| III.3 | Sample preparation of $Zn_xMn_{1-x}Fe_2O_4$ series..... | 75 |
| III.4 | Characterization of $Zn_xMn_{1-x}Fe_2O_4$ nanoparticles..... | 76 |
| III.4.1 | X-ray diffraction analysis..... | 76 |
| III.4.2 | Analysis of TEM micrographs and EDX spectra..... | 83 |
| III.4.3 | Determination of hydrodynamic diameter..... | 86 |
| III.4.3.1 | Dynamic light scattering method (DLS)..... | 86 |
| III.4.3.2 | Particle to particle analysis method (NTA)..... | 87 |
| III.4.4 | Determination of zeta potention and pH of $Zn_xMn_{1-x}Fe_2O_4$ nanoparticles..... | 89 |
| III.4.5 | Influence of chemical composition on IR spectra..... | 90 |
| III.4.6 | Influence of chemical composition on the magnetic properties..... | 92 |
| III.5 | Conclusions..... | 94 |
| | References..... | 95 |
| Chapter IV. | Experimental results - Functionalization of $Zn_xCo_{1-x}Fe_2O_4$ and $Zn_xMn_{1-x}Fe_2O_4$ series. Hemolysis tests..... | 99 |
| IV.1 | Functionalization study of $Zn_xCo_{1-x}Fe_2O_4$ and $Zn_xMn_{1-x}Fe_2O_4$ ($0 < x < 1$) magnetic nanoparticles..... | 99 |
| IV.1.2 | Characterization of $Zn_xCo_{1-x}Fe_2O_4$ and $Zn_xMn_{1-x}Fe_2O_4$ ($0 < x < 1$) functionalized nanoparticles..... | 101 |
| IV.1.2.1 | Study of the particle size by means of transmission electron microscopy..... | 101 |
| IV.1.2.2 | Study of hydrodynamic diameter..... | 105 |
| IV.1.2.3 | Zeta potential..... | 110 |
| IV.1.2.4 | Determination of the molecular structure by IR spectroscopy..... | 111 |
| IV.2 | Interaction of magnetic nanoparticles with the blood-hemolysis test..... | 117 |
| IV.3 | Conclusions..... | 124 |
| | References..... | 124 |
| | General conclusions..... | 126 |
| | Annex 1..... | 129 |
| | Annex 2..... | 130 |
| | Annex 3..... | 131 |
| | Annex 4..... | 132 |

This thesis summary retains the numbering of chapters and paragraphs of the thesis as well as the numbering of the figures and tables.

Introduction

The gold standard in the treatment of malignancies is currently a triad represented by chemotherapy, radiotherapy and surgery. In some types of cancers, this triad is nowadays completed by targeted therapies represented by monoclonal antibodies. Despite this varied therapeutic arsenal cancer mortality is still high, a justification for the continuous research of new therapeutic modalities.

Drug delivery systems are designed to improve the pharmacological and therapeutic properties of drugs, by conveying the drug to the site of interest. Once at the site of interest the goal would be for the drug to be activated only by in response to certain specific stimuli.

The aim of this thesis was focused on the synthesis and characterization of nano-sized magnetic systems ($Zn_xCo_{1-x}Fe_2O_4$ and $Zn_xMn_{1-x}Fe_2O_4$, ($x = 0, 0.2, 0.4, 0.6, 0.8$ and 1), their functionalization using the layer by layer method (LBL) by means of two polyelectrolytes (PAH and PAA) and testing their interaction with blood (hemolysis test). The interest for the study of these materials is justified by numerous applications reported in the medical literature such as targeted drug transport, nuclear magnetic resonance contrast agents and hyperthermia. Chapter I of this study presents some general concepts regarding: the state of research, the principle of targeted transport of drugs and the main classes of magnetic nanoparticles with potential application in drug delivery. The second chapter gives a brief description of the techniques of structural study and of the techniques used for describing the magnetic properties of the nanoparticles. Here we also describe possible methods currently used for the functionalization of nanoparticles with an emphasis on the method of layer by layer deposition. Chapter III details the method of synthesis of the $Zn_xCo_{1-x}Fe_2O_4$ and $Zn_xMn_{1-x}Fe_2O_4$ ($0 < x < 1$) nanoparticles series that we used and the results obtained from XRD, TEM and EDX, DLS, NTA, zeta potential and VSM measurements. Chapter IV is dedicated to nanoparticles functionalization using the LBL method with the two polyelectrolytes, PAH and PAA and to the verification of the biocompatibility of these nanoparticles using a hemolysis test.

Chapter I

Current status of research on the methods of synthesis and the practical applications of nanosized drug delivery systems

1.1 Nanotechnology

Nanotechnology is a multidisciplinary scientific field that involves knowledge of physics and chemistry as well as biology and engineering on the phenomena that occur at the nanometer scale. Immediate applications have already been developed in semiconductor, information technology but also in medicine field [1].

1.2 Current status of research in nanoparticulate systems

Most studies concerning the synthesis of magnetic nanoparticles used for drug delivery have been focused on magnetite or maghemite, due to the low toxicity of iron. Research has also been conducted on other types of nanoparticles such as MgFe_2O_4 , MnFe_2O_4 , FePt , CoFe_2O_4 [2], this area being in continuous development.

1.3 Methods for synthesis of nanostructured systems

Studies have shown that the method of synthesis and the shape of the nanoparticles obtained determine their domain of applicability.

For a better control of their size distribution, shape and degree of agglomeration of nanocrystallites, wet synthesis methods are superior compared to physical ones. It turned out that the method of synthesis influences also the magnetic properties of the ferrite particles. Among the most commonly used synthesis techniques based on a reaction in an aqueous medium to prepare nanocrystalline ferrite particles are: microemulsions technique, sol-gel, hydrothermal method and co-precipitation.

1.3.1 Co-precipitation method

Due to its simplicity and also to its low price, co-precipitation represents the most commonly used wet synthesis technique. During this process the mixed metal oxide with magnetic properties is prepared. An example could be MFe_2O_4 , where $\text{M}^{2+} =$

Mn, Fe, Co, Cu, Zn, is a divalent metal. The nature of the precipitating agent has a significant influence on the morphology of ferrite nanopowders synthesized by co-precipitation method.

1.3.2 Microemulsion method

Microemulsion represents a colloidal system in which one of the two insoluble solutions is dispersed in the form of fine droplets with a diameter of less than 100 nm, in the second liquid phase.

1.3.3 Sol-gel method

Sol-gel technique is a method of synthesis including several steps in which the precursor dissolved in a suitable chosen solvent is converted to the corresponding crystalline oxide through a series of physical and chemical processes. Generally, precursors used by sol-gel method are metal alkoxides and metal salts.

1.3.4 Hydrothermal method

The hydrothermal method is carried out by thermal treatment at temperatures of up to 200°C under high pressure of metal hydroxide suspension obtained by treatment with alkali, or NH₃ solution up to a certain pH of the salt solution containing metal ions corresponding to the pursued oxide system. The formation of oxide particles in the hydrothermal treatment is based on the mechanism of dissolution - precipitation.

1.4 Applications of nanoparticles in medicine - targeted drug delivery

Modern medicine began in 1885 with the discovery of vaccines and techniques for obtaining medicinal plants in the late nineteenth century. The effectiveness of many of the substances used as drugs today are based on their effect on the target molecules located on the membrane or cytoplasm of the aggressor.

Targeted drug delivery originally developed around cancer chemotherapy. The first system of nano-scale drug transport was achieved with lipid micelles, first described in 1960, which then received the name of liposomes. In 1976, Langer and Folkman [3] have demonstrated for the first time controlled release of the drug from nanoparticles, and Leserman et al (1980) created the first targeted liposomes [4]. Besides liposomes, many authors, including Pridgen, in 2007, studied the use of polymeric nanoparticles,

dendrimers, polymer conjugates, protein transporters or inorganic nanoparticles as delivery systems.

1.4.1 The principle of magnetic drug delivery

Targeted drug delivery systems can be controlled so that delivery takes place in the region of interest without affecting healthy neighboring tissue. A controlled transport of the drug in order to eradicate the tumor could be achieved by applying a magnetic field [5].

In magnetic targeted therapy, a cytotoxic drug is attached to a biocompatible magnetic nanoparticle carrier. These types of complexes - biocompatible ferrofluids, are injected into the patient through the circulatory system. After injection of the particles, external magnetic field gradients are used to concentrate the complex formed in the area of interest. Following the application of the magnetic field, the vessel will have a paramagnetic response caused most probably by hemoglobin. At the same time there will be a diamagnetic response as blood proteins contain atoms of carbon, hydrogen, oxygen but also nitrogen. These two answers will be much lower compared with the response of magnetic nanoparticles. Regarding the type of optimal magnetic field for this type of application, it was concluded that a magnetic field gradient provides the force necessary to drive the particles into the area of interest.

The effectiveness of the therapy depends on the physical parameters such as field strength or the magnetic properties of the particles as well as on the hydrodynamic and physiological parameters (concentration of ferrofluid used, the route of administration, etc.).

1.4.2 Groups of nanoparticles used in magnetic drug delivery

The first successful pre-clinical tests of nanoparticles based on iron are attributed to Alexiou et al [6], which established the parameters of this type of nanoparticles targeting after intra-arterial administration. They used external magnetic fields to determine the accumulation of nanoparticles at the level of pelvic limb where the tumor was induced. Colloidal ferrofluid was formed by iron oxides and hydroxides in order to produce aggregates of nanoparticles encapsulated in a polymeric matrix of starch, for stability and to provide binding sites for the methotrexate (MTX). After 3 months of

observation there was no longer detected any histological residual tumor in the test group.

Most of the studies used Ni oxides in hybrid composite with Co or Fe. In these studies Ni nanoparticles served either as inducers of magnetic hyperthermia, drug delivery platforms or direct inducers of apoptosis [7].

Of interest are also the nanoparticles based on cobalt due to their high magnetization (160 and 68 emu/g for Co ferrite elements and Co respectively). Co ferrite was used in the synthesis of nanoparticles that were to be internalized into target cells such as stem cells that would then be guided to the desired active site via an external magnetic field [8].

For medical applications, in addition to the mandatory requirement, that these nanoparticles must be biocompatible, they must also be stable. In this regard several stabilizing agents (*capping agents*) were proposed [9]. Le Guevel et al [10] used citrate dialysis to increase the stability of Mn-Zn nanoparticles, followed by their functionalization, and embedding the drug on their surface afterwards (doxorubicin).

Chapter II

Methods of characterization and functionalization of nanoparticles

II.1 Characterization techniques

The correlation between experimental parameters used to obtain these nanostructures and their functional properties, deliberately targeted to a specific application, can be established only through a laborious and complete characterization methodology.

II.1.1 The method of X-ray diffractometer

X-ray diffraction is a method to investigate the structure of crystalline solids in order to identify the component phases and to determine lattice parameters.

In the case of the nanoparticles studied in this work powder diffractograms were recorded in 2θ geometry at room temperature using X'pert Pro MPD diffractometer (University of Saarland). The cathode ray tube provides a Cu-K α radiation ($\lambda = 1.54\text{\AA}$). A tube voltage of 45kv, a current of 40 mA and a step of 0.02° were used.

II.1.2 Transmission electron microscopy (TEM) and energy dispersive X-ray (EDX)

Given the size of the objects that we want to observe optical microscopy was not sufficient. Because of this reason, transmission electron microscopy has established itself in recent years as the basic technique to characterize nanostructures in general and nanoparticles in particular and we used it too, given the nature of this study.

In addition to the projection image obtained from the transmitted beam and addition to the information derived from the study of the diffraction pattern, another possible application of a focused beam of electrons is embodied in a method known as energy dispersive X-ray (EDX).

The morphology of the samples studied in this work was obtained by electron microscopy JOEL Model JEM 2010 ($U_{\text{acc}}=200\text{kV}$) (University of Saarland).

II.1.3 Dynamic light scattering (DLS)

Dynamic light scattering is a method of obtaining information on the average size of nanoparticles by studying the dynamics of Brownian motion of particles in solution. In the case of this technique we obtain information about the average size of nanoparticles from solution derived from the study of the light scattering due to the interaction between the laser beam and the particles in the sample studied.

To determine the hydrodynamic diameter of these studied magnetic nanoparticles series we used a Zetasizer Nano ZS device from Malvern Instruments from the Department of Physical Chemistry, University of Saarland.

II.1.4 Particle with particle analyzing method (NTA)

Compared with the dynamic light scattering technique described above, that can bring information about the average size of nanoparticles from the studied solution, the NTA technique provides a size distribution of nanoparticles by analyzing the sample in real time.

The sample in the form of suspension is placed on an opaque background while a laser beam is used so that the nanoparticles can be directly viewed by an optical microscope.

Measurements of hydrodynamic particle diameter through this particle by particle analysis method (NTA) were performed

using a Nano Sight LM20 device (Nano Sight, United Kingdom), in the endowment of the Solid State Department of the Faculty of Physics, "A.I.Cuza" University Iasi, Romania.

II.1.5 Method for determining zeta potential

Colloidal particles dispersed in a solution are electrically charged due to their ionic characteristics and to its dipolar properties. Zeta potential is considered to be the difference in potential between the dispersion medium and the constant layer of fluid attached to the dispersed particles; and is considered that when the potential is closer to 0, the particles tend to agglomerate.

Measuring the stability of colloidal solutions required the use of a Zetasizer 3000 HSA device from Malvern Instruments Company in endowment of the Department of Physical Chemistry from the University of Saarland, Germany.

In our case, zeta potential measurements were carried out in order to check the stability of the nanoparticles in an aqueous medium and to confirm their functionalization.

II.1.6 Fourier Transform Infrared Spectroscopy

The principle of this method is based on measuring the absorption of infrared radiation by the sample being analyzed. IR absorption spectrum bands are specific to the type of chemical bonds in a molecule, thus realizing the identification of molecular and structural components.

In our case, Fourier transform infrared spectroscopy was used to confirm both the spinel structure of the synthesized nanoparticles and to confirm their functionalization after using the layer-by-layer (LBL) method.

The IR spectrum of the synthesized particles was recorded with a FTIR spectrometer from JASCO 660 Plus belonging to the Laboratory of Inorganic Chemistry from the "A.I.Cuza" University, in the field of $4000\text{-}400\text{cm}^{-1}$ with a resolution of 4 cm^{-1} .

In the case of functionalized nanoparticles a Perkin Elmer FTIR spectrometer was used to record the IR spectra between 750 and 4000 cm^{-1} with a resolution of 4 cm^{-1} (Department of Physical Chemistry, University of Saarland, Germany). Sample preparation consisted of pipetting a colloidal solution on ZnSe slides followed by drying the drops in a stream of nitrogen.

II.1.7 Vibrating sample magnetometer (VSM)

Vibrating sample magnetometer technique consists in measurement of the magnetic properties of materials. Vibrating sample magnetometer (VSM) is a versatile device that allows precise measurements of the magnetic moment in a uniform or variable magnetic field, depending on the temperature and the crystallographic axis orientation.

For these measurements we used a Lake Shore Model 7300 vibrating sample magnetometer (VSM) from the Institute for New Materials, Saarbrücken, Germany.

II.2 Methods for functionalization of nanoparticles for medical applications

Small particles have found numerous applications, especially in diagnostic purposes but also in therapeutic applications, at least in *in vitro* research. Nanoparticles can be injected intravenously, and then the flow of blood ensures they are conveyed to the region of interest, or another option is to inject the particles directly in the desired region. Any of these options requires that the particles do not form aggregates. The formation of such aggregates would cause embolisms which would lead to blocking their dissemination in the bloodstream and may cause unwanted effects on normal tissues. To prevent these effects it is necessary to discuss methods that can be used to produce a stable suspension of nanoparticles.

Clinical research results suggest that functionalization of nanoparticles with specific recognition chemical compounds, results in real multifunctional nanoparticles. These functionalized nanoparticles have an increased effectiveness and functionalization is accompanied by a significant reduction of systemic side effects.

II.2.1 Layer-by-layer method (LbL)

The technique of layer-by-layer self-assembly based on polyelectrolytes represents one of the newest methods of obtaining structures in the nanometer range. Proposed by G. Decher in the early 1990s, the method consists of the use of polymers solutions that carry opposite charges on different structures. The original description of the LBL technique consists in immersing the substrate surface in alternative polyelectrolyte solutions. The surfaces coated by this method can be made of plastic, glass, quartz, silicon,

ceramics, while the layers can be a solution of a polycation (polymer bearing positive charges in aqueous solution) and an aqueous solution of a polyanion (polymer bearing negative charges in aqueous solution). The alternative immersion process continues in this way depending on the number of layers desired. After each adsorption step, the substrate is rinsed several times with water, to remove the excess of polyelectrolyte and dried with a slow stream of nitrogen.

An important reference point in the application of LBL method was the deposition of polymer molecules on aggregates of colloidal particles. This achievement belongs to the group G. Sukhorukov, E. Donath, F. Caruso and H. Mohwald [11], from the Max Planck Institute for Colloids and Interfaces.

Chapter III

Experimental results - Synthesis method and experimental techniques for studying the structural and magnetic properties of the obtained nanostructures

III.1 Obtaining magnetic nanostructures of $Zn_xCo_{1-x}Fe_2O_4$

Ferrite magnetic nanoparticles $Zn_xCo_{1-x}Fe_2O_4$ where $x = 0, 0.2, 0.4, 0.6, 0.8$ and 1 , were prepared using the co-precipitation method in the Department of Physical Chemistry at the University of Saarland - Germany [12].

In the synthesis and dispersion process of $Zn_xCo_{1-x}Fe_2O_4$ ferrite series in water we followed these steps:

1. $NaOH$ (10.16g) was dissolved in 200mL of distilled water at $90^\circ C$.
2. $FeCl_3 \cdot 6H_2O$ (10.81g) was dissolved in 40mL of distilled water at $70^\circ C$;
3. $ZnCl_2$ (Xg) and $CoCl_2 \cdot 6H_2O$ (Yg) were dissolved in 8mL of distilled water at $70^\circ C$ and 1mL of HCl.

Components obtained at steps 1, 2 and 3 were mixed while stirring for 60 minutes at $90^\circ C$ followed by 60 min at $25^\circ C$ and then sedimented by means of a permanent magnet. Finally the sediment underwent a three step washing with 200 mL of distilled water.

4. Stabilization with 3ml HNO_3 solution dissolved in 51.7 mL of distilled water with stirring at $80^\circ C$;

5. $Fe(NO_3)_3 \cdot 9H_2O$ (8.482g) was dissolved in 60mL of distilled water at 70°C;
6. $ZnCl_2$ (X/2g) and $CoCl_2 \cdot 6H_2O$ (Y/2g) were dissolved in 8.5mL of distilled water at 70°C.

After the solutions had reached 80°C, respectively 70°C, they were combined and stirred for 30 minutes at 80°C, followed by 30 minutes of cooling the resulting mixture. Using a magnet the powder was retained and the surplus of HNO_3 was washed.

For use in the medical field ferrofluids must meet requirements relating to stability over time. In order to ensure this, ferrofluids underwent dialysis, in a solution of sodium citrate (0.01M) for 7 days. This was followed by 7 days of dialysis with distilled water to remove the excess of citrate from the surface of the nanoparticles.

III.2 Characterization of $Zn_xCo_{1-x}Fe_2O_4$ magnetic nanoparticles series

III.2.1 The results of microstructure by X-ray diffraction

The analysis of the recorded diffractograms confirmed the formation of cubic spinel structure for all samples. The results illustrate the increase in lattice parameter with the increase of Zn. This increase can be attributed to the substitution of Co cation that has a smaller ionic radius (0.78 Å) than the zinc cation, which has a larger ionic radius (0.82 Å) [13]. Comparing the results obtained for the experimental lattice constants with the theoretically ones, by calculating the cation distribution, it can be seen that preserves the same trend of increasing with increasing zinc concentration.

Crystallite size was determined using Scherrer's formula, applying first a Lorentzian deconvolution for the diffraction peaks for each sample. Following the analysis, it has been observed that the average crystallite size decreased from 15nm to 7nm with the increase in concentration of zinc from 0 to 1. Arumugan et al [14] showed that substitution of zinc plays an important role in reducing the size of the crystallites.

For our system, $Zn_xCo_{1-x}Fe_2O_4$, the cation distribution (Table III.2.1) can be expressed as follows:

$$(Zn_{x-a}^{2+}Co_{1-x-b}^{2+}Fe_{a+b}^{3+})[Zn_b^{2+}Co_a^{2+}Fe_{2-(a+b)}^{3+}]O_4^{2-} \quad (III.5)$$

Table III.2.1 Crystallite diameter (d_{XRD}), experimental lattice constant (a_{exp}) and theoretical lattice constant (a_{th}), the distribution of cations, oxygen positional parameter (u), inversion parameter (i) tetrahedral position radius (r_A) and octahedral position radius (r_B) cation-oxygen bond distance tetrahedral position (R_A) and octahedral position (R_B) for $Zn_xCo_{1-x}Fe_2O_4$ series

| | d_{XRD} (nm) | a_{exp} (Å) | a_{th} (Å) | Cation distribution | u (Å) | i | r_A (Å) | r_B (Å) | R_A (Å) | R_B (Å) |
|--|----------------|---------------|--------------|--|---------|------|-----------|-----------|-----------|-----------|
| CoFe ₂ O ₄ | 15 | 8.351 | 8.322 | (Co _{0.2} ²⁺ Fe _{0.8} ³⁺)[Co _{0.8} ²⁺ Fe _{1.6} ³⁺] | 0.3835 | 0.80 | 0.5040 | 0.5900 | 1.884 | 1.970 |
| Zn _{0.2} Co _{0.8} Fe ₂ O ₄ | 12 | 8.361 | 8.340 | (Zn _{0.1} ²⁺ Co _{0.1} ²⁺ Fe _{0.8} ³⁺)[Zn _{0.1} ²⁺ Co _{0.7} ²⁺ Fe _{1.2} ³⁺] | 0.3835 | 0.80 | 0.5080 | 0.5945 | 1.888 | 1.974 |
| Zn _{0.4} Co _{0.6} Fe ₂ O ₄ | 10 | 8.364 | 8.362 | (Zn _{0.14} ²⁺ Co _{0.05} ²⁺ Fe _{0.81} ³⁺)[Zn _{0.26} ²⁺ Co _{0.55} ²⁺ Fe _{1.19} ³⁺] | 0.3832 | 0.81 | 0.5089 | 0.6022 | 1.888 | 1.982 |
| Zn _{0.6} Co _{0.4} Fe ₂ O ₄ | 10 | 8.371 | 8.391 | (Zn _{0.1} ²⁺ Fe _{0.90} ³⁺)[Zn _{0.5} ²⁺ Co _{0.4} ²⁺ Fe _{1.1} ³⁺] | 0.3822 | 0.90 | 0.5010 | 0.6175 | 1.881 | 1.997 |
| Zn _{0.8} Co _{0.2} Fe ₂ O ₄ | 7 | 8.414 | 8.417 | (Zn _{0.08} ²⁺ Fe _{0.92} ³⁺)[Zn _{0.72} ²⁺ Co _{0.2} ²⁺ Fe _{1.08} ³⁺] | 0.3816 | 0.92 | 0.4988 | 0.6284 | 1.878 | 2.008 |
| ZnFe ₂ O ₄ | 7 | 8.434 | 8.439 | (Zn _{0.11} ²⁺ Fe _{0.89} ³⁺)[Zn _{0.89} ²⁺ Fe _{1.11} ³⁺] | 0.3814 | 0.90 | 0.5010 | 0.6355 | 1.881 | 2.015 |

From Table III.2.1 we can see that the calculated oxygen positional parameter (u) approaches the ideal value of 0.375\AA characteristic of the tetrahedral position, the difference between values being due to the conditions of synthesis. Lattice parameter values indicate that the studied series present a partial inverse spinel structure due to the distribution of divalent cations both in tetrahedral as well as in the octahedral positions.

The increase of r_B can be explained by the fact that although the cation Zn^{2+} prefers the tetrahedral position, in our case it can be found also in the octahedral positions. The substitution of the cobalt ions with those of zinc determine an increase of the r_B value, due to the large ionic radius (0.82\AA) of Zn^{2+} compared to that of Co^{2+} (0.78\AA) [13]. The same pattern of growth is also present for r_A for samples with $x = 0, 0.2,$ and 0.4 . In their case, increasing the amount of Zn^{2+} cations present in tetrahedral position determines an increase of r_A . For samples with $x = 0.6$ and 0.8 , the values of tetrahedral radius position recorded a decreasing effect which can be corroborated with the decrease of Zn^{2+} cations in the tetrahedral position. The sample $x = 1$, ZnFe_2O_4 , presents an r_A value equivalent to that of the sample $x = 0.6$, the explanation being given by the fact that in the tetrahedral position of both samples the amount of Zn^{2+} cations is the same.

III.2.2 Study of microstructure and chemical composition using transmission electron microscopy (TEM) and energy dispersive X-ray spectroscopy (EDX)

The distribution by size of nanoparticles was determined counting 60 particles from the recorded TEM images. Observations on the shape and particle size distribution are shown in Figure III.2.5. For the $\text{Zn}_x\text{Co}_{1-x}\text{Fe}_2\text{O}_4$ series the diameters resulting from the transmission electron microscopy analysis had values between 9 - 16nm, dimensions that are consistent with the results obtained from the X-ray diffraction measurements, suggesting that the particles are mainly consist of a single magnetic domain.

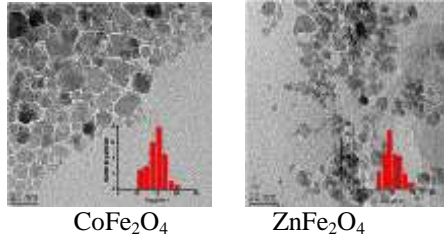


Figure III.2.5 TEM micrographs and size distribution of $Zn_xCo_{1-x}Fe_2O_4$ magnetic nanoparticles

Analyzing TEM images corresponding to the $Zn_xCo_{1-x}Fe_2O_4$ series one can say that these have a narrow size distribution and low agglomeration, a necessary requirement for their application in any biomedical field. EDX analysis confirmed the presence of Fe, Zn and Co metal for all the $Zn_xCo_{1-x}Fe_2O_4$ series ferrites.

III.2.3 The determination of the hydrodynamic diameter of the powder of $Zn_xCo_{1-x}Fe_2O_4$ series

III.2.3.1 Dynamic light scattering method (DLS)

In Table III.2.3 the corresponding hydrodynamic diameter values of the $Zn_xCo_{1-x}Fe_2O_4$ series are presented. The size as determined by means of the DLS technique is much higher than that determined by XRD and TEM techniques.

Table III.2.3 Hydrodynamic diameter values for the $Zn_xCo_{1-x}Fe_2O_4$ ferrites series

| | $d_{hidro}(nm)$ |
|---------------------------|-----------------|
| $CoFe_2O_4$ | 41.5± 1.8 |
| $Zn_{0.2}Co_{0.8}Fe_2O_4$ | 45.4± 2.3 |
| $Zn_{0.4}Co_{0.6}Fe_2O_4$ | 49.8± 2.5 |
| $Zn_{0.6}Co_{0.4}Fe_2O_4$ | 39.9± 0.1 |
| $Zn_{0.8}Co_{0.2}Fe_2O_4$ | 45.2± 3.0 |
| $ZnFe_2O_4$ | 41.2± 0.4 |

This difference in size is due to the fact that the particles of the $Zn_xCo_{1-x}Fe_2O_4$ series dispersed in water have a tendency to agglomerate and form aggregates and this fact is leading to a significant increase of the measured size [15].

III.2.3.2 Particle with particle analysis method (NTA)

Following the NTA analysis we found that the size distribution for each sample component of Zn-Co series, for the three investigated times (30s, 40s and 60s), presents approximately the same trend. This result denotes the stable behavior of nanoparticles.

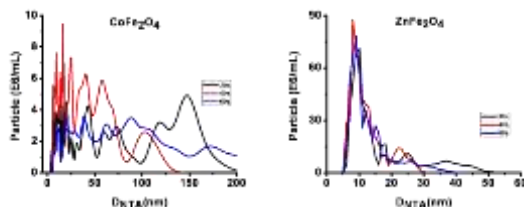


Figure III.2.7 Distribution by size of nanoparticles resulting from the NTA of $Zn_xCo_{1-x}Fe_2O_4$ ($0 < x < 1$) magnetic nanoparticles

Unlike the dynamic light scattering (DLS) method, the analysis of the particles with NTA particle analysis method, allows direct observation of the sample and can also provide the approximate concentrations of particles. Both methods have shown good measurement accuracy and relatively narrow distributions for all analyzed samples.

III.2.5 Zeta Potential determination for colloidal dispersions

This subchapter reports data concerning the zeta potential values for each sample as well as the pH of the fluid in which the magnetic nanoparticles were dispersed, in our case distilled water.

Table III.2.5 The values of the zeta potential and the pH for aqueous dispersions of nanoparticles of ferrite series $Zn_xCo_{1-x}Fe_2O_4$

| | ZetaPotential (mV) | pH |
|--|-----------------------|------|
| CoFe ₂ O ₄ | -44.8± 6.0 | 6.92 |
| Zn _{0.2} Co _{0.8} Fe ₂ O ₄ | -53.8± 12.6 | 7.08 |
| Zn _{0.4} Co _{0.6} Fe ₂ O ₄ | -44.1± 12.0 | 7.06 |
| Zn _{0.6} Co _{0.4} Fe ₂ O ₄ | -49.3± 0.5 | 7.09 |
| Zn _{0.8} Co _{0.2} Fe ₂ O ₄ | -51.8± 1.4 | 6.97 |
| ZnFe ₂ O ₄ | -51.2± 4.4 | 6.91 |

Analyzing the results of zeta potential measurements, it can be concluded that the $Zn_xCo_{1-x}Fe_2O_4$ series ferrites present values lower than -30mV.

From these measurements it can be stated that the colloidal system presents a stable behavior and a pH value proper for biomedical applications.

III.2.6 Influence of chemical composition on IR spectra

In Figure III.2.8 the FTIR spectra corresponding to the $Zn_xCo_{1-x}Fe_2O_4$ ferrites series after synthesis are presented. Absorption bands located between 3402 and 3394cm^{-1} are found to be due to O-H stretching vibration that corresponds to the hydroxyl group attached to the surface by hydrogen bonding to iron oxide.

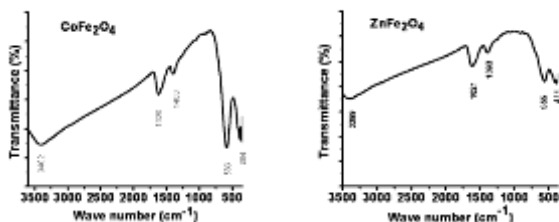


Figure III.2.8 FTIR spectra of $Zn_xCo_{1-x}Fe_2O_4$ magnetic nanoparticles with $x=0$ and 1

Following the analysis, the presence of citrate on the surface of the particles is confirmed by the occurrence of significant peaks specific to the deprotonated carboxyl group, between 1621 and 1616cm^{-1} . The frequency band around 600cm^{-1} wavenumber is assigned to the metal-oxygen vibration specific to the tetrahedral positions ($M_{\text{th}}-\text{O}$), while around the wavenumber of 400cm^{-1} is identified the specific vibrations of metal-oxygen specific to the octahedral positions ($M_{\text{oh}}-\text{O}$) [16].

The wavelength number corresponding to the first frequency band, ν_1 , decreases with increasing the content of Zn. This variation can be attributed to the increase in the length of cation-oxygen bond. The results indicate a weakening of the metal-oxygen tetrahedral positions due to the substitution of Fe^{3+} ions with those of Zn^{2+} . Substitution with Zn^{2+} ions in the tetrahedral position determines Fe^{3+} ions to migrate to the octahedral position, which leads to an increase in the cation-oxygen bond length in the

tetrahedral position (a drop in the frequency band, ν_1). Regarding the substitution with Zn^{2+} ions, the ν_2 frequency band, increases approximately linearly toward higher wave numbers for the entire studied series. This indicates strengthening of the metal-oxygen bond in octahedral position due to the displacement of Fe^{3+} ions from tetrahedral to the octahedral position. These results are consistent with several studies conducted on mixed Cu-Zn ferrites [17] as well as on Mg-Zn ones[18].

Table III.2.4 The positions of IR absorption bands (ν_1 and ν_2), the values of force constants corresponding to tetrahedral (k_A) and octahedral (k_B) positions for the $Zn_xCo_{1-x}Fe_2O_4$ series

| | ν_1 (cm^{-1}) | ν_2 (cm^{-1}) | k_A ($dyne/cm^2$) | k_B ($dyne/cm^2$) |
|---------------------------|--------------------------|--------------------------|--------------------------|--------------------------|
| $CoFe_2O_4$ | 583 | 384 | $1.43 \cdot 10^5$ | $1.15 \cdot 10^5$ |
| $Zn_{0.2}Co_{0.8}Fe_2O_4$ | 581 | 388 | $1.46 \cdot 10^5$ | $0.91 \cdot 10^5$ |
| $Zn_{0.4}Co_{0.6}Fe_2O_4$ | 577 | 399 | $1.49 \cdot 10^5$ | $0.97 \cdot 10^5$ |
| $Zn_{0.6}Co_{0.4}Fe_2O_4$ | 579 | 386 | $1.45 \cdot 10^5$ | $0.93 \cdot 10^5$ |
| $Zn_{0.8}Co_{0.2}Fe_2O_4$ | 575 | 392 | $1.42 \cdot 10^5$ | $0.97 \cdot 10^5$ |
| $ZnFe_2O_4$ | 565 | 411 | $1.45 \cdot 10^5$ | $1.07 \cdot 10^5$ |

With increasing zinc content a variation of force constants can be observed, especially for the two positions. This variation suggests a weakening of the interatomic bond.

III.2.7 The influence of the chemical composition on the magnetic properties (VSM)

$Zn_xCo_{1-x}Fe_2O_4$ nanoparticles have a spinel structure in which the unit cell has a face-centered cubic symmetry (FCC).

Magnetization curves of the samples, recorded at room temperature, are shown in Figure III.2.9. They show a ferrimagnetic behavior for samples with $x = 0$ and 0.2 and a superparamagnetic behavior for samples with $x = 0.4, 0.6, 0.8$ and 1.

Saturation magnetization decreased from the value of 62.4 emu/g to 20.7 emu/g when the concentration of zinc increased from $x = 0$ to $x = 1$. The values of the coercive field decreased with increasing concentration of zinc. From Table III.2.5 we can see that

the calculated and experimental values of magneton number decreases with increasing zinc content in the sample.

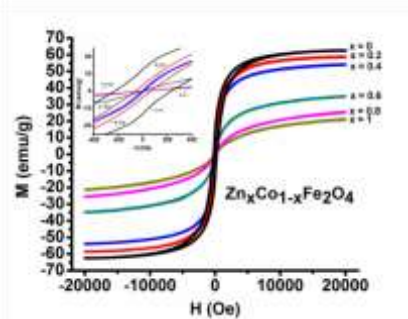


Figure III.2.9 The hysteresis cycles at room temperature, of the powder sample series for $Zn_xCo_{1-x}Fe_2O_4$, with $x = 0, 0.2, 0.4, 0.6, 0.8, 1$ content of Zn

This can be explained by the preference of divalent cations for tetrahedral position, while the decrease of the magnetic moment can be explained by means of the Yafet-Kittel angle. Regarding zinc ferrite magnetic properties, these are found to be strongly influenced by the particle size.

Table III.2.5 Saturation magnetization (M_s), the magnetic moment of subnetworks A and B (M_A , M_B), magneton number (n_B) and Yafet-Kittel (YK) angle for the $Zn_xCo_{1-x}Fe_2O_4$ series of nanoparticle

| | M_s (emu/g) | H_c (Oe) | M_A | M_B | n_B (th) | n_B (exp) | YK (degree) |
|---------------------------|---------------|------------|-------|-------|---------------|----------------|----------------|
| $CoFe_2O_4$ | 62.4 | 250.16 | 4.60 | 8.40 | 3.800 | 2.726 | 29.29 |
| $Zn_{0.2}Co_{0.8}Fe_2O_4$ | 58.8 | 49.96 | 4.30 | 8.10 | 3.800 | 2.587 | 31.76 |
| $Zn_{0.4}Co_{0.6}Fe_2O_4$ | 54.1 | - | 4.20 | 7.60 | 3.400 | 2.403 | 29.68 |
| $Zn_{0.6}Co_{0.4}Fe_2O_4$ | 34.8 | - | 4.50 | 6.70 | 2.200 | 1.607 | 24.29 |
| $Zn_{0.8}Co_{0.2}Fe_2O_4$ | 25.2 | - | 4.60 | 6.00 | 1.400 | 1.212 | 14.38 |
| $ZnFe_2O_4$ | 20.7 | - | 4.45 | 5.55 | 1.100 | 1.01 | 10.33 |

As it is known, zinc ferrite in its solid form is considered to be a normal spinel where Zn^{2+} ions occupies almost exclusively tetrahedral (A) interstices while the Fe^{3+} ions occupies octahedral (B) interstices. In the case of spinels with inverted structure the

Zn^{2+} cations are oriented also towards octahedral interstices, whereas Fe^{3+} ions occupy both octahedral as well as tetrahedral interstices. So high magnetization of zinc ferrite nanoparticles is due to the strong AB interaction between Fe ions from B interstices and Fe ions that were forced to migrate to A interstices when the nanoparticles were synthesized. In our case, the high magnetization can be explained through the variation of cation distribution which occurs when increasing zinc concentration.

III.3 Preparation of $Zn_xMn_{1-x}Fe_2O_4$ sample series

The preparation protocol used to obtain the samples of the $Zn_xMn_{1-x}Fe_2O_4$ ($x = 0, 0.2, 0.4, 0.6, 0.8$ and 1) series is based on the chemical precipitation method [19]. Given that the resulting pH (approximately 2) is not suitable for biomedical applications, the solution was subjected to dialysis.

III.4 Characterization of $Zn_xMn_{1-x}Fe_2O_4$ magnetic nanoparticles

III.4.1 X-ray diffractograms analysis

XRD diffractograms of magnetic material are presented in a summarized fashion in Figure III.4.1.

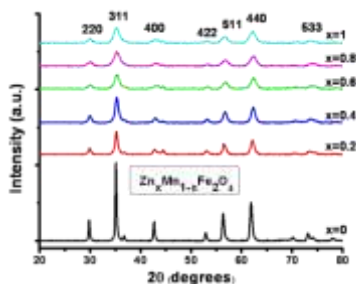


Figure III.4.1 XRD diffractograms of $Zn_xMn_{1-x}Fe_2O_4$ series

As in the case of the $Zn_xCo_{1-x}Fe_2O_4$ series, there is also a variation in the lattice parameter (a), of the Zn-Mn series. These values can be assigned to the substitution of the Mn cation that has a larger ionic radius (0.93\AA) than the zinc cation that has a smaller ionic radius (0.82\AA) [13, 16]. Theoretical lattice parameter, a_{th} , presents the same trend as the variation of the experimental lattice parameter, a_{exp} .

Table III.4.1 Crystallite diameter (d_{XRD}) experimental lattice constant (a_{exp}) and theoretical (a_{th}) lattice constant, the distribution of cations, oxygen positional parameter (u), inversion parameter (i) tetrahedral position radius (r_A) and octahedral position radius (r_B) cation-oxygen bond distance for the tetrahedral position (R_A) and the octahedral one (R_B) for $\text{Zn}_x\text{Mn}_{1-x}\text{Fe}_2\text{O}_4$ series

| | $d_{\text{XRD}}(\text{nm})$ | $a_{\text{exp}}(\text{Å})$ | $a_{\text{th}}(\text{Å})$ | Cation distribution | $u(\text{Å})$ | i | $r_A(\text{Å})$ | $r_B(\text{Å})$ | $R_A(\text{Å})$ | $R_B(\text{Å})$ |
|---|-----------------------------|----------------------------|---------------------------|--|---------------|------|-----------------|-----------------|-----------------|-----------------|
| MnFe_2O_4 | 22 | 8.460 | 8.461 | $(\text{Mn}_{0.95}^{2+}\text{Fe}_{0.05}^{3+})[\text{Mn}_{0.05}^{2+}\text{Fe}_{1.95}^{3+}]$ | 0.3913 | 0.05 | 0.652 | 0.557 | 2.032 | 1.937 |
| $\text{Zn}_{0.2}\text{Mn}_{0.8}\text{Fe}_2\text{O}_4$ | 14 | 8.440 | 8.443 | $(\text{Zn}_{0.18}^{2+}\text{Mn}_{0.76}^{2+}\text{Fe}_{0.06}^{3+})[\text{Zn}_{0.02}^{2+}\text{Mn}_{0.04}^{2+}\text{Fe}_{1.94}^{3+}]$ | 0.3908 | 0.06 | 0.639 | 0.558 | 2.019 | 1.938 |
| $\text{Zn}_{0.4}\text{Mn}_{0.6}\text{Fe}_2\text{O}_4$ | 13 | 8.420 | 8.426 | $(\text{Zn}_{0.35}^{2+}\text{Mn}_{0.57}^{2+}\text{Fe}_{0.08}^{3+})[\text{Zn}_{0.05}^{2+}\text{Mn}_{0.03}^{2+}\text{Fe}_{1.92}^{3+}]$ | 0.3901 | 0.08 | 0.625 | 0.559 | 2.005 | 1.939 |
| $\text{Zn}_{0.6}\text{Mn}_{0.4}\text{Fe}_2\text{O}_4$ | 10 | 8.400 | 8.411 | $(\text{Zn}_{0.5}^{2+}\text{Mn}_{0.38}^{2+}\text{Fe}_{0.12}^{3+})[\text{Zn}_{0.1}^{2+}\text{Mn}_{0.02}^{2+}\text{Fe}_{1.88}^{3+}]$ | 0.3893 | 0.12 | 0.610 | 0.562 | 1.990 | 1.942 |
| $\text{Zn}_{0.8}\text{Mn}_{0.2}\text{Fe}_2\text{O}_4$ | 9 | 8.390 | 8.412 | $(\text{Zn}_{0.45}^{2+}\text{Mn}_{0.19}^{2+}\text{Fe}_{0.36}^{3+})[\text{Zn}_{0.35}^{2+}\text{Mn}_{0.01}^{2+}\text{Fe}_{1.64}^{3+}]$ | 0.3867 | 0.36 | 0.572 | 0.585 | 1.952 | 1.965 |
| ZnFe_2O_4 | 7 | 8.430 | 8.431 | $(\text{Zn}_{0.2}^{2+}\text{Fe}_{0.8}^{3+})[\text{Zn}_{0.8}^{2+}\text{Fe}_{1.2}^{3+}]$ | 0.3823 | 0.80 | 0.512 | 0.626 | 1.892 | 2.006 |

The average crystallite size decreased from 22nm (± 0.2 nm) to 7 nm (± 0.2 nm) proportional to the increase of the content of zinc, from 0 to 1. An explanation of this behavior would be that higher zinc concentration in solution during synthesis produces an increase in the reaction rate, which favors the formation of ultra-fine particles of ferrite mixed.

Zinc ions occupying the octahedral position can alter the cations distribution, resulting in the modification of structural and magnetic properties of the $Zn_xMn_{1-x}Fe_2O_4$ nanoparticles.

The results presented in Table III.4.1 indicates a preference of each cation (Zn^{2+} , Mn^{2+} and Fe^{3+}) for the two positions. Following the analysis, the structure of nanoparticles is a partial inverse spinel, characterized by an inversion parameter value between $0 < i < 1$.

Preference of Zn^{2+} cations from the $Zn_xMn_{1-x}Fe_2O_4$ series for the tetrahedral position is confirmed by the higher values recorded for tetrahedral position radius (r_A) compared with those for $Zn_xCo_{1-x}Fe_2O_4$ series.

According to the r_A values for the entire series of Zn-Mn ferrites, we obtained lower values for octahedral position radius (r_B). A secondary explanation for the r_A and r_B values would be that the ionic radius of Mn^{2+} (0.93Å) is higher than that of Zn^{2+} (0.82Å), and as it can be seen from cation distribution shown in Table III.4.1, most of the Zn^{2+} and Mn^{2+} cations are found in the tetrahedral position.

III.4.2 Analysis of TEM micrographs and EDX spectra

TEM results have confirmed the XRD data, for all corresponding samples analyzed series, and provide details of the crystalline grain morphology.

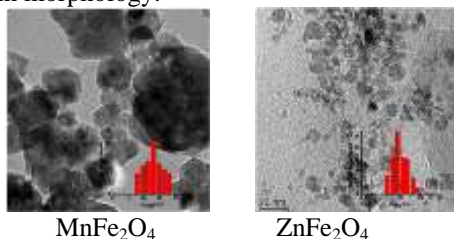


Figure III.4.5 TEM micrographs and size distribution of $Zn_xMn_{1-x}Fe_2O_4$ nanoparticles for sample $x = 0$ and 1

As in the case of the previously analyzed series, $Zn_xCo_{1-x}Fe_2O_4$, Zn-Mn ferrites series present dimensions in the nanometer range which suggests that the particles are mostly formed by single magnetic domain.

We have found that the analyzed magnetic particles are relatively well dispersed and they are almost spherical. EDX analysis confirmed the presence of Fe, Zn and Mn in the case of the all analyzed samples.

III.4.3 Determination of hydrodynamic diameter for $Zn_xMn_{1-x}Fe_2O_4$ ferrite

III.4.3.1 Dynamic light scattering method (DLS)

Just as in the case of the Zn-Co ferrite series, the size of the samples as determined by DLS technique is much higher than that determined by XRD and TEM techniques. Comparing the two analyzed series, Zn-Co and Zn-Mn ($0 < x < 1$), we can see that the recorded values for the hydrodynamic diameter determined by DLS technique does not exceed 50 nm, except for the manganese ferrite where the diameter was about 99.5 nm.

Table III.4.6 *Hydrodynamic diameter values for $Zn_xMn_{1-x}Fe_2O_4$ series*

| | $d_{hydro}(nm)$ |
|--|-----------------|
| MnFe ₂ O ₄ | 99.5 ± 2.9 |
| Zn _{0.2} Mn _{0.8} Fe ₂ O ₄ | 47.8 ± 0.6 |
| Zn _{0.4} Mn _{0.6} Fe ₂ O ₄ | 38.5 ± 0.5 |
| Zn _{0.6} Mn _{0.4} Fe ₂ O ₄ | 41.1 ± 2.3 |
| Zn _{0.8} Mn _{0.2} Fe ₂ O ₄ | 44.1 ± 2.5 |
| ZnFe ₂ O ₄ | 41.2 ± 0.4 |

The relatively large difference of dimension, registered from the XRD, TEM and DLS techniques for our magnetic nanoparticles can be explained by the fact that their dispersion in water favors the formation of aggregates giving rise to an increase in the determined size.

III.4.3.2 Particle with particle analysis method (NTA)

Analyzing the results we found that the dimensions obtained by applying particle with particle analysis method were smaller, the range of the size distribution being closer to the values obtained by transmission electron microscopy (9-23 nm).

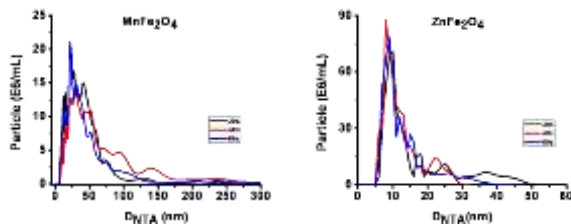


Figure III.4.7 Distribution by size of nanoparticles resulting from the NTA measurements for $x=0$ and 1 from $Zn_xMn_{1-x}Fe_2O_4$ ($0 < x < 1$) series

Because there were no significant variations in the size of the analysis at three different times, it can be stated that the samples show a stable behavior over time.

III.4.4 Determination of zeta potential and pH of the $Zn_xMn_{1-x}Fe_2O_4$ particles

All samples of Zn-Mn series have values greater than the negative limit, -30mV , indicating that the samples analyzed are stable and the value of the pH is suitable for biomedical applications.

III.4.5 Influence of chemical composition on IR spectra

As a result of the analysis of the IR spectra recorded for samples of Zn-Mn series, one can observe a wide band of absorption in the range of 3426 cm^{-1} - 3391 cm^{-1} present in each spectrum. This band confirmed the presence of water traces. Also, a wide band of absorption can be observed around the wavenumber of 1621 cm^{-1} - 1616 cm^{-1} , band which is characteristic of deprotonated carboxyl group, thus confirming the presence of citrate ions on the surface of the nanoparticles. Absorption bands of low intensity that can be seen between 400 cm^{-1} and 600 cm^{-1} are associated with vibration modes of metal - oxygen bonds.

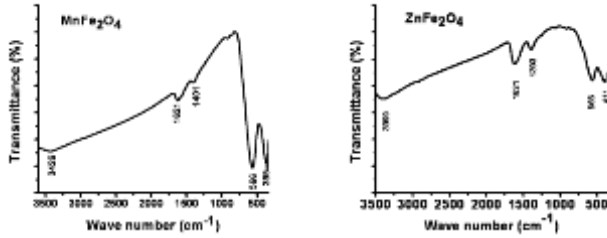


Figure III.4.8 FTIR spectra of samples $x = 0$ and 1 of $Zn_xMn_{1-x}Fe_2O_4$ series

After examining the position of the absorption bands we found a trend of decreasing ν_1 with increasing zinc content in the sample. Substitution of manganese ions caused migration of the majority of the Fe^{3+} ions from the tetrahedral to the octahedral position. But with increasing Zn content of the sample a slight increase is also recorded in the content of Fe^{3+} in tetrahedral position. This slight increase can be related to the decrease in the R_A , which can be interpreted as a strengthening of the metal-oxygen bond in the tetrahedral position.

Table III.4.8 The positions of IR absorption bands (ν_1 and ν_2), the values of force constants corresponding to tetrahedral (k_A) and octahedral (k_B) positions for the $Zn_xMn_{1-x}Fe_2O_4$ series

| | ν_1 (cm^{-1}) | ν_2 (cm^{-1}) | k_A ($dyne/cm^2$) | k_B ($dyne/cm^2$) |
|--|--------------------------|--------------------------|--------------------------|--------------------------|
| MnFe ₂ O ₄ | 566 | 395 | $1.34 \cdot 10^5$ | $0.92 \cdot 10^5$ |
| Zn _{0.2} Mn _{0.8} Fe ₂ O ₄ | 588 | 430 | $1.49 \cdot 10^5$ | $1.09 \cdot 10^5$ |
| Zn _{0.4} Mn _{0.6} Fe ₂ O ₄ | 569 | 412 | $1.44 \cdot 10^5$ | $1.01 \cdot 10^5$ |
| Zn _{0.6} Mn _{0.4} Fe ₂ O ₄ | 571 | 390 | $1.49 \cdot 10^5$ | $0.90 \cdot 10^5$ |
| Zn _{0.8} Mn _{0.2} Fe ₂ O ₄ | 568 | 407 | $1.47 \cdot 10^5$ | $1.01 \cdot 10^5$ |
| ZnFe ₂ O ₄ | 565 | 411 | $1.40 \cdot 10^5$ | $1.07 \cdot 10^5$ |

The high values of metal-oxygen length R_B (Table III.4.1) denote strong metal-oxygen bonds in the octahedral position. As it can be seen, the force constants, both k_A and k_B , varies according to the cations distribution (Table III.4.1) in both positions, the tetrahedral (A), respectively, the octahedral (B) one. The registered decrease suggests the weakening of interatomic bonds.

III.4.6 Influence of chemical composition on the magnetic properties of $Zn_xMn_{1-x}Fe_2O_4$ ferrite nanoparticles

Analyzing the magnetization curves we found that the synthesized particles with $x = 0.2, 0.4, 0.6, 0.8$ and 1 do not present remanent magnetization and are not characterized by hysteresis. These results confirmed that the particles present a superparamagnetic behavior. For $x = 0$, Mn ferrite, a coercive field value equal to 49.89 Oe has been observed, which indicates the ferrimagnetic nature of these particles. Looking at the shape of the magnetization curves we noted that the magnetic properties of Zn-Mn ferrite series components are dependent on the content of zinc in the sample.

In Table III.4.9 the saturation magnetization values are presented and as it can be seen they decreased with increasing zinc content.

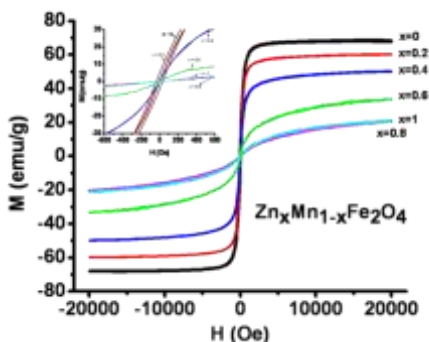


Figure III.4.9 Hysteresis cycles at room temperature for powder samples with $x = 0, 0.2, 0.4, 0.6, 0.8, 1$ Zn content

Saturation magnetization values have decreased from 67.7 emu/g, value registered for manganese ferrite, until 20.7 emu/g for zinc ferrite.

As a result of decrease in Mn concentration, a decrease in the magnetization recorded for the M_A tetrahedral position is noted, as well as for the octahedral M_B position. The reason for the

decrease of the magnetic moment can be explained on the basis of the Yafet-Kittel angle.

Table III.4.9 Saturation magnetization (M_s), the magnetic moment of subnetworks A and B (M_A , M_B), magnetron number (N_B) and Yafet-Kittel (YK) angle of $Zn_xMn_{1-x}Fe_2O_4$ series

| | M_s (emu/g) | H_c (Oe) | M_A | M_B | n_B (th) | n_B (exp) | YK (degree) |
|---------------------------|---------------|------------|-------|-------|---------------|----------------|----------------|
| $MnFe_2O_4$ | 67.7 | 49.89 | 5.00 | 10.00 | 5.00 | 2.82 | 38.57 |
| $Zn_{0.2}Mn_{0.8}Fe_2O_4$ | 60.06 | - | 4.10 | 9.90 | 5.80 | 2.53 | 47.93 |
| $Zn_{0.4}Mn_{0.6}Fe_2O_4$ | 50.02 | - | 3.25 | 9.75 | 6.50 | 2.16 | 56.28 |
| $Zn_{0.6}Mn_{0.4}Fe_2O_4$ | 33.47 | - | 2.50 | 9.50 | 7.00 | 1.58 | 64.55 |
| $Zn_{0.8}Mn_{0.2}Fe_2O_4$ | 20.64 | - | 2.75 | 8.25 | 5.50 | 1.00 | 62.96 |
| $ZnFe_2O_4$ | 20.73 | - | 4.00 | 6.00 | 2.00 | 1.01 | 33.38 |

These low magnetic moments can be explained by the spin arrangement, namely the presence of the canting effect in the B position regarding the distortion of A position.

Chapter IV

Experimental results - Functionalization of $Zn_xCo_{1-x}Fe_2O_4$ and $Zn_xMn_{1-x}Fe_2O_4$ series. Hemolysis tests

IV.1 Functionalization study of $Zn_xCo_{1-x}Fe_2O_4$ and $Zn_xMn_{1-x}Fe_2O_4$ ($0 < x < 1$) magnetic nanoparticles

During the experiments, the method of deposition of PAH and PAA layers have followed the following steps [19, 20]:

1. 25mg PAH was dissolved in 9 mL distilled water;
2. The solution thus formed was ultrasonicated for 20 min, followed by a process of magnetic stirring;
3. 9mL of ferrofluid was gradually dripped over the polycation solution;
4. The solution was left to stir 12h at room temperature in the dark;
5. After the 12h stirring the solution of magnetic nanoparticles coated with polycation undergoes a dialysis

treatment for 48 hours in order to get rid of the excess of polycation;

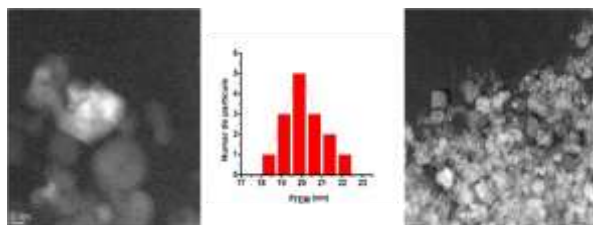
6. To deposit the next layer of polyanion (PAA) the same steps are used. The number of steps can be repeated until the desired number of layers of polymer is reached.

To verify the effectiveness of the method we used several techniques such as the FTIR spectrum analysis and TEM micrographs as well as the measurement of zeta potential and the hydrodynamic diameter, through both methods DLS and NTA.

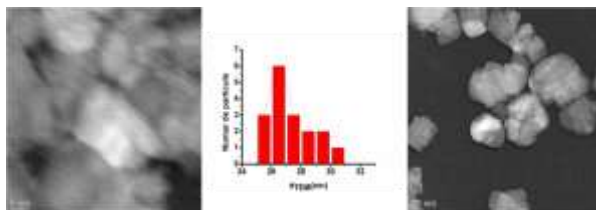
IV.1.2 Characterization of $Zn_xCo_{1-x}Fe_2O_4$ and $Zn_xMn_{1-x}Fe_2O_4$ ($0 < x < 1$) functionalized nanoparticles

IV.1.2.1 Study of the particle size by means of transmission electron microscopy

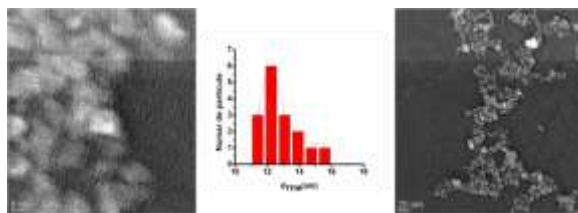
Particle size distribution after the coating process was processed with *ImageJ*. The presence of the polymer is confirmed by the difference in the signal observed around the nanoparticles. After analyzing the images we were able to estimate an increase of about 3-4 nm.



(PAH/PAA/PAH) - CoFe₂O₄



(PAH/PAA/PAH) - MnFe₂O₄



(PAH/PAA/PAH) – $ZnFe_2O_4$

Figure IV.1.3 TEM micrographs after the coating process for the two series of ferrite nanoparticles a. $Zn_xCo_{1-x}Fe_2O_4$ and b. $Zn_xMn_{1-x}Fe_2O_4$ ($0 < x < 1$)

20nm scale images corresponding to the two synthesized series shows that the covered $Zn_xMn_{1-x}Fe_2O_4$ has a lower tendency to agglomeration than $Zn_xCo_{1-x}Fe_2O_4$ series. In addition, it is expected that the particles covered with the two polyelectrolytes, PAH and PAA, did not affect the particle morphology.

IV.1.2.2 Hydrodynamic diameter study

In Table IV.1.1 are the average values of the corresponding hydrodynamic diameter of the nanoparticles after each polyelectrolyte layer deposited and the measurement error.

Hydrodynamic diameter by DLS measurements showed that in an aqueous dispersion medium magnetic nanoparticles coexist as small aggregates. Measured diameters can also be affected by surface-polymer bonds that slow down the diffusion and increase the apparent size of the particles or possible aggregates.

Table IV.1.2 Hydrodynamic diameter values for a) $Zn_xCo_{1-x}Fe_2O_4$ and b) $Zn_xMn_{1-x}Fe_2O_4$

| a. | MNP (nm) | PAH – MNP (nm) | (PAH/PAA) – MNP (nm) | (PAH/PAA/PAH) –MNP(nm) |
|---------------------------|----------------|-------------------|-------------------------|---------------------------|
| $CoFe_2O_4$ | 41.5 ± 1.8 | 63.4 ± 0.2 | 105.1 ± 1.6 | 144.1 ± 0.8 |
| $Zn_{0.2}Co_{0.8}Fe_2O_4$ | 45.4 ± 2.3 | 66.9 ± 0.9 | 113.5 ± 0.4 | 136.2 ± 0.6 |
| $Zn_{0.4}Co_{0.6}Fe_2O_4$ | 49.8 ± 2.5 | 65.2 ± 0.5 | 80.5 ± 0.4 | 138.8 ± 0.4 |
| $Zn_{0.6}Co_{0.4}Fe_2O_4$ | 39.9 ± 0.1 | 67.7 ± 0.3 | 90.4 ± 0.8 | 121.6 ± 0.2 |
| $Zn_{0.8}Co_{0.2}Fe_2O_4$ | 45.2 ± 3.0 | 66.8 ± 1.3 | 88.8 ± 1.5 | 117.9 ± 0.6 |
| $ZnFe_2O_4$ | 41.2 ± 0.4 | 62.1 ± 1.1 | 91.3 ± 0.3 | 136.1 ± 0.2 |

| b. | MNP (nm) | PAH – MNP (nm) | (PAH/PAA) – MNP (nm) | (PAH/PAA/PAH) – MNP(nm) |
|--|-------------|-------------------|-------------------------|----------------------------|
| MnFe ₂ O ₄ | 99.5 ± 2.9 | 135.5 ± 0.7 | 173.9 ± 1.8 | 202.9 ± 8.2 |
| Zn _{0.2} Mn _{0.8} Fe ₂ O ₄ | 47.8 ± 0.6 | 72.9 ± 1.4 | 105.3 ± 2 | 124.3 ± 4.5 |
| Zn _{0.4} Mn _{0.6} Fe ₂ O ₄ | 38.5 ± 0.5 | 67.7 ± 1.9 | 87.9 ± 0.4 | 119.9 ± 2.2 |
| Zn _{0.6} Mn _{0.4} Fe ₂ O ₄ | 41.1 ± 2.3 | 66.6 ± 2.1 | 88.9 ± 1 | 119.6 ± 0.4 |
| Zn _{0.8} Mn _{0.2} Fe ₂ O ₄ | 44.1 ± 2.5 | 83.6 ± 1.8 | 90.4 ± 2.4 | 137.4 ± 2.3 |
| ZnFe ₂ O ₄ | 41.2 ± 0.4 | 62.1 ± 1.1 | 91.3 ± 0.3 | 136.1 ± 0.2 |

Since the synthesis of nanoparticles aimed their possible application in targeted drug delivery, more accurate information about the hydrodynamic diameter are necessary. Therefore, as a complementary measurement to the measurements obtained through the DLS method, we performed a particle with particle analysis method (NTA) [21]. NTA measurements showed that the functionalized nanoparticles corresponding to both series, Zn-Co and Zn-Mn, have the same trend of the size distribution for all the three periods of time examined. This indicates that these nanoparticles have a stable behavior over time.

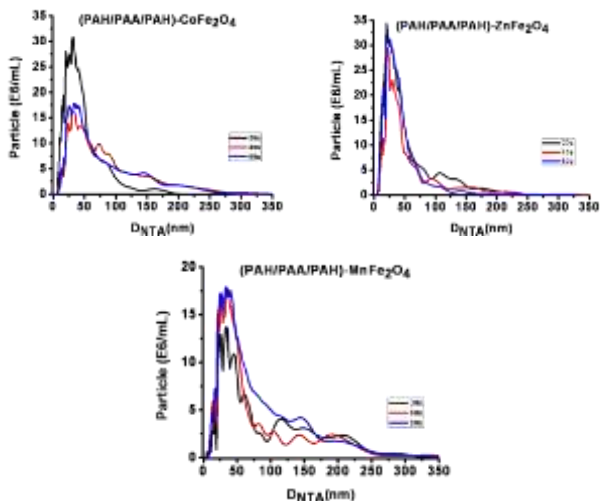


Figure IV.14 Distribution by size through NTA of functionalized magnetic nanoparticles a) Zn_xCo_{1-x}Fe₂O₄ and b) Zn_xMn_{1-x}Fe₂O₄ (0 < x < 1)

The results also illustrated that through the NTA method the values were much lower than those obtained through the DLS method. In the case of functionalized nanoparticles corresponding to the Zn-Co series sizes in the range of 21nm - 31nm were detected, while for the Zn-Mn series sizes ranged from 21nm - 36 nm.

IV.1.2.3 Zeta potential

As a result of measurements we found that the value of zeta potential changed after each deposition step, both in the case $Zn_xCo_{1-x}Fe_2O_4$ and $Zn_xMn_{1-x}Fe_2O_4$ series where $x = 0, 0.2, 0.4, 0.6, 0.8$ and 1 . It should be noted that the pH of all samples was between 6-7, a pH necessary for biomedical applications.

IV.1.2.4 Determination of the molecular structure by IR spectroscopy

To verify the presence of the two polymers on the surface of magnetic nanoparticles corresponding to the two series, we initially recorded the IR spectra of the two polymers used. Figure IV.1.4 present the spectra of the two polymers, PAH and PAA (Annex 1).

In Figure IV.1.5 a) and b) are shown the FTIR spectra corresponding to the two series synthesized, *Zn-Co* and *Zn-Mn*, compared to the polymers spectra. Comparing the FTIR spectra of the coated nanoparticles with the first layer (PAH) with that of the polymer one can simply say that the adsorption of the polymer on the surface of magnetic nanoparticles with citrate was achieved in both series $Zn_xCo_{1-x}Fe_2O_4$ and $Zn_xMn_{1-x}Fe_2O_4$.

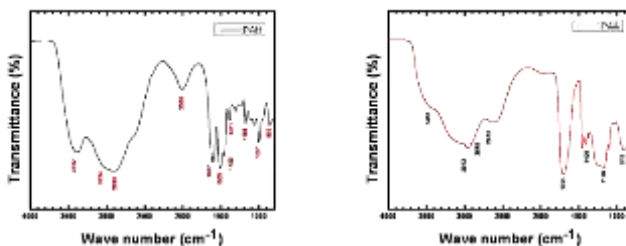


Figure IV.1.2.4 FTIR spectra of the two polymers used, PAH and PAA

Analyzing the sample spectrum after the deposition of PAA layer (PAH/PAA-MNP) we concluded that the adsorption of polyanion was successful.

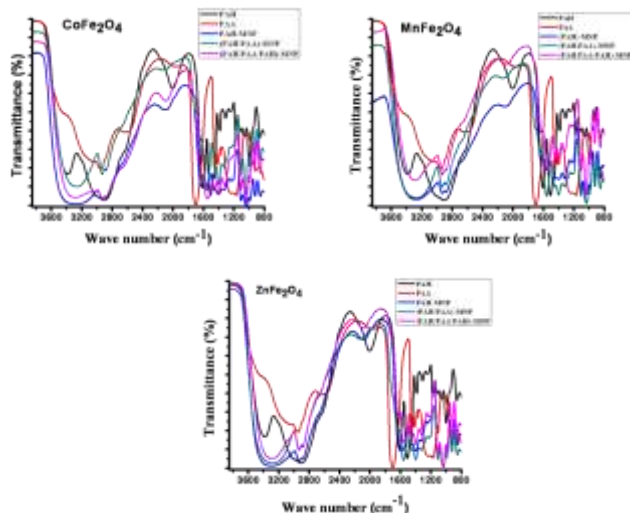


Figure IV.1.2.5 FTIR spectra corresponding to the two functionalized series and of the two polymers

Thus, the FTIR spectrum is a combination of all bands of vibration of the entire multi-layer system.

IV.2 Interaction of magnetic nanoparticles with the blood - hemolysis test

If the nanoparticles are not biocompatible their interaction with the red blood cells will have an acute toxic effect on the erythrocytes that will result in the lysis of these cells [22]. Given the immediate and long-term interaction of nanoparticles with blood, we considered it important to test the hemolysis induced by functionalized nanoparticles as a last step in the validation protocol for the future applications.

The hemolysis test, as shown by its name is based on the evaluation of lytic effect of nanoparticles on red blood cells.

Secondary to cell lysis, hemoglobin, which is in high concentrations in red blood cells, is released in the dilution medium

in which the hemolysis test is carried out. Therefore measurements of hemoglobin concentration in the serum can bring information about the degree of hemolysis induced by nanoparticles [23].

In our case we decided to use the hemolysis test to compare the lytic effect of uncoated nanoparticles with that of the coated ones, the premise from which we have started being that the functionalization of nanoparticles is a way to enhance the biocompatibility of nanoparticles, not just a way to make them useful in targeted drug delivery applications.

All samples were processed using the same protocol:

1. 3 mL blood + 1 mL FF (magnetic nanoparticles dispersed in aqueous medium);
2. 30 min incubation at a temperature of 37°C;
3. 5 min centrifugation at 3000 rot/min;
4. Dilution of the supernatant in 0.9% NaCl solution (20 mL supernatant resulted from centrifugation of the sample + 3 mL of 0.9% NaCl solution).

Samples resulted from phase 4 of the protocol were subsequently subjected to spectrophotometric investigation. For this purpose we used a UV-VIS GBC Model CINTRA spectrophotometer, located in the laboratory of Inorganic Chemistry at the “Al.I.Cuza” University, Iasi.

After analyzing the obtained spectra we observed that samples containing magnetic nanoparticles present a higher level of hemoglobin compared to the control sample without nanoparticles. This highlighted an increase in the phenomenon of hemolysis following the addition of magnetic fluid.

As it can be seen in Figure IV.2.4 the degree of hemolysis induced by $Zn_xMn_{1-x}Fe_2O_4$ series is significantly lower compared with the one of Zn-Co series, which can be explained by the high level of biocompatibility of the combination of zinc-manganese compared to the level of biocompatibility of zinc-cobalt combination.

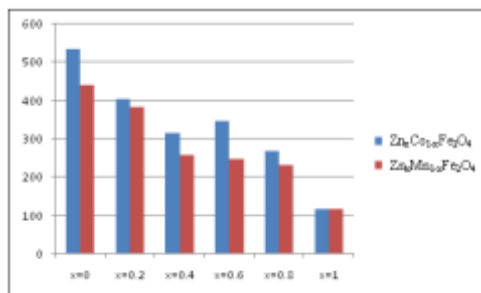


Figure IV.2.4 Comparison of the degree of hemolysis induced by nanoparticles of the two studied series

We have also conducted comparisons between members of the same series before and after functionalization with LBL method (PAH/PAA/PAH). After functionalization we registered a significant decrease in the degree of hemolysis compared to the uncoated nanoparticles. An explanation for the decrease in the degree of hemolysis is that the presence of polyelectrolytes on the nanoparticles surface prevents direct interaction of nanoparticles with blood, recognized by the body as non-self and attacked by the immune system.

Conclusions

The aim of this work consisted in the synthesis and characterization of water-based magnetic systems, $Zn_xCo_{1-x}Fe_2O_4$ and $Zn_xMn_{1-x}Fe_2O_4$ ($0 < x < 1$), with possible applications in medicine and to present the results of experimental studies concerning their functionalization and their influence over hemoglobin. These magnetic nanoparticles were synthesized by co-precipitation method from the corresponding metal chlorides in the sodium hydroxide solution. The stability of the nanoparticles was obtained by using sodium citrate ions resulting in a pH of about 7.

Samples of synthesized magnetic nanoparticles were characterized in terms of dimensional, structural and magnetic properties - highlighting the necessary features of their application in targeted drug delivery.

We also studied, the functionalization of the two series of nanoparticles using the method of deposition layer-by-layer (LbL).

The characterization of the nanoparticles obtained by means of the algorithms described revealed that these are valid method for obtaining functionalized nanoparticles. Also, the NTA measurements done at three different time intervals from the moment of synthesis have shown that the functionalized nanoparticles belonging to the two series, Zn-Co, respectively Zn-Mn present a similar tendency for the size distribution. This means that the functionalized nanoparticles are stable in time.

We analyzed the interaction of nanoparticles before and after functionalization with the blood. We have estimated the degree of hemolysis induced by the presence of magnetic nanoparticles before and after functionalization using UV-VIS spectroscopy.

- As a result it has been observed that by functionalizing of the nanoparticles these structures became more difficult to recognize by the immune system, which translates into a lower degree of induced hemolysis.

We conclude by saying that the functionalization is a method to improve the biocompatibility of nanoparticles but it can also be used to support the possible surface binding of a drug in order to facilitate the targeted transport of drugs.

Selective bibliography

- [1]Coey J.M.D., *Magnetism and magnetic materials*, Ed. Cambridge University Press, New York (2010)
- [2]Prijic S, Sersa G, *Magnetic nanoparticles as targeted delivery systems in oncology*, Radiol Oncol 45(1), 1-16 (2011)
- [3]Langer R, Folkman J, *Polymers for the sustained release of proteins and other macromolecules*, Nature (London) 263, 797-800 (1976)
- [4]Leserman L.D, Barbet J, Kourilsky F, Weinstein J.N, *Targeting to cells of fluorescent liposomes covalently coupled with monoclonal antibody or protein A*, Nature 288, 602-604 (1980)
- [5]Goodwin D.A, Meares C.F, *Advances in pretargeting biotechnology*. Biotechnol Adv 19, 435-450 (2001)
- [6]Alexiou C, Arnold W, Klein R.J, et al. *Locoregional cancer treatment with magnetic drug targeting*, Cancer Res 60(23), 6641-8 (2000)
- [7]Ahamed M, Akhtar M.J, Siddiqui M.A, et al, *Oxidative stress mediated apoptosis induced by nickel ferrite nanoparticles in cultured A549 cells*, Toxicology 283(2-3), 101-8 (2011)
- [8]Baldi G, Bonacchi D, Franchini M.C, et al. *Synthesis and coating of cobalt ferrite nanoparticles: a first step toward the obtainment of new magnetic nanocarriers*, Langmuir 23(7), 4026-8 (2007)
- [9]Gherca D, Pui A, Ciornei M, **Cojocariu A**, Nica V, Caltun O.F, *Synthesis, characterization and magnetic properties of MFe_2O_4 ($M=Co, Mg, Mn, Ni$) nanoparticles using ricin oil as capping agent*, J MagnMagn Mater 324, 3906-3911(2012)
- [10]Le Guével X. et al., *Synthesis and characterization of superparamagnetic nanoparticles coated with fluorescent gold nanoclusters*, J Nanopart Res 14, 727-737(2012)
- [11]Caruso F, Caruso R.A, Möhwald H, *Nanoengineering of inorganic and hybrid hollow spheres by colloidal templating*, Science 282, 1111-1114 (1998)
- [20]Doaga A, **Cojocariu A.M**, Amin W, Heib F, Bender P, Hempelmann R, Caltun O.F, *Synthesis and characterizations of manganese ferrites for hyperthermia applications*, accepted at Mat ChemPhys (2013)

- [13] Sharma A, Parmar K, Kornala R.K, Negi N.S, *Magnetic and dielectric properties of $\text{Co}_x\text{Zn}_{1-x}\text{Fe}_2\text{O}_4$ synthesized by metallo-organic decomposition technique*, IJAET, Nov. (2012)
- [14] Arulmurugan R, Jeyadevan B, Vaidyanathan G, Sendhilnathan S, *Effect of zinc substitution on Co–Zn and Mn–Zn ferrite*
- [15] Chen J.P, Yang P.C, Ma Y.H, Wu T, *Characterization of chitosan magnetic nanoparticles for in situ delivery of tissue plasminogen activator*, Carbohyd Polym 84, 364-372 (2011)
- [16] **Cojocariu A. M.**, Soroceanu M, Hrib L, Nica V, Caltun O. F, *Microstructure and magnetic properties of substituted (Cr, Mn) – cobalt ferrite nanoparticles*, Mater Chem Phys 135, 728-732 (2012)
- [17] Zaki H.M, Dawoud H.A, *Far-infrared spectra for copper–zinc mixed ferrites*, Physica B 405, 4476- 4479 (2010)
- [18] Mohammed K.A, Al-Rawas A.D, Gismelseed A.M, Sellai A, Widatallah H.M, Yousif A, Elzain M.E, Shongwe M, *Infrared and structural studies of $\text{Mg}_{1-x}\text{Zn}_x\text{Fe}_2\text{O}_4$ ferrites*, Physica B 407, 795–804 (2012)
- [19] **Cojocariu A. M.**, Doaga A, Amin W, Bender P, Hempelmann R, Caltun O.F, *Synthesis and functionalization of magnetic nanoparticles with possible application in drug delivery systems*, Dig J Nanomater Bios, 8 (2), 519 – 527 (2013)
- [20] A. Doaga, **A.M. Cojocariu**, C.P. Constantin, R. Hempelmann, O.F. Caltun, *Magnetic Nanoparticles for Medical Applications: Progress and Challenges, AIP Conference Proceedings* (2013)
- [21] Montes-Burgos I, Walczyk D, Hole P, Smith J, Lynch I, Dawson K, *Characterisation of nanoparticle size and state prior to nanotoxicological studies*, J Nanopart Res 12, 47–53 (2010)
- [22] Arora S, Rajwade J.M, Paknikar K.M, *Nanotoxicology and in vitro studies: The need of the hour*, Toxicol Appl Pharm 258, 151–165(2012)
- [23] Wu W, Chen B, Cheng J, Wang J, Xu W, Liu L, Xia G, Wei H, Wang X, Yang M, Yang L, Zhang Y, Xu C, Li J, *Biocompatibility of Fe_3O_4 /DNR magnetic nanoparticles in the treatment of hematologic malignancies*, Int J Nanomed 5, 1079–1084 (2010)

Annex 1

Polyallylamine hydrochloride (PAH)

| Wave number | Functional groups | Type of vibration |
|-------------|------------------------------|-----------------------------------|
| 3382 | NH ₃ ⁺ | Bond vibration |
| 3024 | N-H | Bond vibration |
| 2896 | C-H din CH ₂ | Symmetrical bond vibration |
| 2008 | NH ₃ ⁺ | “overtone” |
| 1607 | | Symmetrical and |
| 1505 | NH ₃ ⁺ | asymmetrical stretching vibration |
| 1455 | CH ₂ | Scissoring vibration |
| 1381 | C-H | Bending vibration |
| 1188 | | |
| 1001 | C-C | Bond vibration |
| 855 | NH ₃ ⁺ | Oscillation vibration |

Polyacrylic acid (PAA)

| Wave number | Functional groups | Type of vibration |
|-------------|----------------------------------|---------------------------------|
| 3452 | O-H | Bond vibration |
| 2943 | | Symmetrical and |
| | | asymmetrical stretching |
| 2875 | C-H | vibration from the |
| | | methylene group CH ₂ |
| 1704 | C=O | Bond vibration |
| 1408 | CH ₂ -CO ⁻ | Bending vibration |
| 1166 | C-C | Bond vibration |
| 915 | C-H | Out of plane bending vibration |

Publications in ISI Thomson indexed journals:

- 1. Cojocariu A.M.**, Soroceanu M., Hrib L., Nica V., Caltun O.F., *Microstructure and magnetic properties of substituted (Cr, Mn) – cobalt ferrite nanoparticles*, Mater Chem Phys 135, 728-732(2012) (Impact Factor – 2.234, AIS – 0.628)
- 2. Gherca D., Pui A., Ciornei M., Cojocariu A.**, Nica V., Caltun O.F., *Synthesis, characterization and magnetic properties of MFe_2O_4 ($M=Co, Mg, Mn, Ni$) nanoparticles using ricin oil as capping agent*, J Magn Magn Mater 324, 3906–3911(2012) (Impact Factor – 1.780, AIS – 0.475)
- 3. Cojocariu A.M.**, Doaga A, Amin W, Bender P, Hempelmann R, Caltun O.F, *Synthesis and functionalization of magnetic nanoparticles with possible application in drug delivery systems*, Dig J Nanomater Bios, 8 (2), 519 – 527 (2013) (Impact Factor – 1.092, AIS – 0.230)
- 4. Doaga A, Cojocariu A.M.**, Amin W, Heib F, Bender P, Hempelmann R, Caltun O.F, *Synthesis and characterizations of manganese ferrites for hyperthermia applications*, accepted for publication at Mat Chem Phys (2013) (Impact Factor – 2.234, AIS – 0.628)
- 5. Doaga A., Cojocariu A.M.**, Constantin C.P., Hempelmann R., Caltun O.F., *Magnetic Nanoparticles for Medical Applications: Progress and Challanges, AIP Conference Proceedings* (ISI indexed)

List of non-ISI publications:

- 1. Constantin Cristin Petrica, Doaga Anamaria, Cojocariu Alina Mihaela**, Dumitru Ioan, Caltun Ovidiu Florin - *Improved Contrast Agents for Magnetic Nuclear Resonance Medical Imaging*, JARP, Vol 2, Nr. Vol 2, No 1 (2011), Al.I.Cuza University Press, 2011, ISBN 2069-7201, pp. 011106- 1-4
- 2. Doaga Anamaria, Constantin Cristin, Cojocariu Alina**, Astefanoaei Iordana, Dumitru Ioan, Caltun Ovidiu F. - *Phenomenological study of the thermal field generated by nanoparticles arrays in hyperthermia as treatment method*, JARP/vol. 2, Nr. Vol.2 No.1 2011, Al.I.Cuza University Press, 2011, ISBN 2067-0451, pp. 011110 -1-4

International conference presentations: 16

National conference presentations: 4